Available online at www.sciencedirect.com
ScienceDirect
Trans. Nonferrous Met. Soc. China 33(2023) 3157−3167
Transactions of Nonferrous Metals Society of China
www.tnmsc.cn

Separation of molybdenite from chalcopyrite with thiolactic acid depressant: Flotation behavior and mechanism

Wei-xin HUANG[1,2], Hong-hu TANG[1,2], Yang CAO[1,2], Ruo-hua LIU[1,2], Wei SUN[1,2]

1. School of Minerals Processing and Bioengineering, Central South University, Changsha 410083, China;
2. Engineering Research Center of Ministry of Education for Carbon Emission Reduction in Metal Resource Exploitation and Utilization, Central South University, Changsha 410083, China

Received 5 May 2022; accepted 20 September 2022

Abstract: The separation of molybdenite and chalcopyrite is a major challenge because of their similar floatability. It is essential to discover a depressant for selectively inhibiting chalcopyrite in a profitable and sustainable way. A novel chalcopyrite depressant, thiolactic acid (TLA), was proposed. The flotation behaviors were studied through micro-flotation and artificial mixed minerals flotation. Micro-flotation experiments indicated that thiolactic acid could significantly suppress chalcopyrite recovery from 81% to 9.7%, along with molybdenite recovery always more than 71%. Artificial mixed minerals flotation experiments showed a distinct separation behavior between chalcopyrite and molybdenite with an optimal Gaudin's selectivity index of 12.9. The reactivity mechanism of TLA on molybdenite and chalcopyrite surfaces was determined by FT-IR, XPS, and AFM with a possible adsorption model presented. The results revealed that —SH and —COOH groups of TLA preferentially occupied the active copper site on chalcopyrite surface, inhibiting subsequent sodium n-butyl xanthate chemisorption.

Key words: thiolactic acid; chalcopyrite; chalcopyrite depressant; Cu−Mo separation

1 Introduction

Molybdenum plays a crucial role in alloy manufacturing, the electronics industry, stainless steel production, chemical catalysts, fertilizer manufacturing, and medical equipment [1−4]. Molybdenite (MoS_2) is a significant mineral of molybdenum resources, accounting for much of the metal's economic viability, which is closely associated with chalcopyrite in the sulfide deposits [5−9]. Normally, molybdenite and chalcopyrite are recovered by bulk flotation and separated from the chalcopyrite−molybdenite bulk concentrate [10−12]. However, the flotation separation of these two minerals is still a major challenge for production, owing to the similar floatability of molybdenite and chalcopyrite and the lack of effective flotation reagents [13].

Depressants play a decisive role in the selective flotation separation reagents for molybdenite and chalcopyrite. In recent decades, many inorganic and organic chalcopyrite depressants have generally been proposed in Table 1. These depressants have been used to amplify the floatability difference and separate molybdenite from chalcopyrite−molybdenite bulk concentrate [14−15]. However, they have not been widely used in industry because of the comprehensive consideration of toxicity, cost, and selectivity [16,17]. Thus, it is worthwhile to discover viable substitute depressants for selectively inhibiting chalcopyrite economically and ecologically.

Thiolactic acid (TLA), also known as 2-mercaptopropionic acid, is a colourless, slightly yellowish liquid that is broadly used in cosmetics, food, and home care. As shown in Fig. 1, thiolactic acid (TLA) contains COOH and SH functional

Corresponding author: Yang CAO, Tel: +86-15084740137, E-mail: caoyang@csu.edu.cn
DOI: 10.1016/S1003-6326(23)66324-1

Table 1 Summary of chalcopyrite depressant

Category	Depressant	Application stage	Dosage
Inorganics	Sodium sulfide [18]	Industry	9−13 kg/t
	Hydrogen peroxide [19]	Industry	800 g/t
	Nokes reagents [19]	Industry	1−2 kg/t
Organic small molecules	*L*-cysteine [20]	Laboratory (Bench-scale actual rock flotation)	25 mg/L
	AHS [13]	Laboratory (Bench-scale actual rock flotation)	150 mg/L
Organic polymer	O-carboxymethyl chitosan [21]	Laboratory (Single pure mineral flotation)	50 mg/L
	Xanthan gum [22]	Laboratory (Artificial mixed single-minerals flotation)	60 mg/L

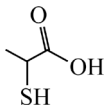

Fig. 1 Molecular structure of thiolactic acid

groups. Previous studies have shown that the —SH functional group could react with metal ions, such as copper, to form Cu—S bond [7,23]. Therefore, TLA has a great potential to be applied in the flotation industry as a chalcopyrite depressant. To date, the feasibility of TLA on the selective separation of chalcopyrite from molybdenite through flotation are still not understood. Moreover, there is a lack of systematic research on the flotation behavior and mechanism from this flotation system, which is particularly important when one considers the upscaling of the process from laboratory tests to industrial applications.

In this study, the effects of TLA on the flotation behavior of both chalcopyrite and molybdenite were investigated via both single-mineral and artificial mixed minerals flotation with sodium n-butyl xanthate (as xanthate is a toxic reagent with potential health and environmental risks [24,25], the use of sodium n-butyl xanthate has always been kept at a low concentration). A concept of Gaudin selectivity index is introduced to confirm the effect of TLA on molybdenite and chalcopyrite separation. The inhibiting mechanism of TLA was studied by Fourier transform infrared spectroscopy (FT-IR), X-ray photoelectron spectroscopy (XPS), and Atomic force microscope (AFM) in detail. A possible adsorption model of TLA on the molybdenite and chalcopyrite surfaces was then proposed. The research results indicated that thiolactic acid was a flexible, economical, and green chalcopyrite depressant in the separation of chalcopyrite−molybdenite. This work offers a better understanding of the depression mechanism of TLA for chalcopyrite, which provides important practical guidance in chalcopyrite−molybdenite separation.

2 Experimental

2.1 Samples and reagents

Chalcopyrite and molybdenite were obtained from Sichuan Province, China. They were characterized using X-ray diffraction (XRD) to ensure that the samples had single phases (Fig. 2). The pure samples were collected by handpicking, pulverized in a ceramic ball mill, crushed, and ground to particle sizes of 37−74 μm before being used for microflotation.

Sodium n-butyl xanthate (SBX), thiolactic acid (TLA), and terpineol were used as the collector, depressant, and frother, respectively. Sodium hydroxide (NaOH) and hydrochloric acid (HCl) were adopted to regulate the pulp pH level. All reagents were in analytical grade, and deionized (DI) water was used throughout the test.

2.2 Flotation experiments

Microflotation was carried out in an XFG flotation machine with spindle speed of 1992 r/min. The flotation processes were as follows: (1) 2 g of pure mineral samples were added to the flotation cell with 40 mL of DI water; (2) NaOH or HCl was used to adjust the pH value; (3) Flotation reagents were added in order and stirred for 3 min, with 3 min interval after each addition; (4) The float and sink fractions were collected, filtered, dried, and weighed to calculate the flotation recovery. Each microflotation test was replicated three times, and the average was calculated to ensure the reproducibility of the results.

Gaudin's selectivity index (SI, I_S), as the convenient measure of two-way separation, denotes

the recovery and rejection between two components. It can better present the selectivity separation of a valuable mineral from gangue [26]. By this definition, SI can represent the quality of separation between molybdenite and chalcopyrite in the presence of TLA. The selectivity index was calculated using the following equation:

$$I_S = \sqrt{\frac{R_m \cdot J_b}{(100-R_m)(100-J_b)}} \quad (1)$$

where R_m is the molybdenite recovery in the flotation concentrate; and J_b is the chalcopyrite recovery in the tailing fraction.

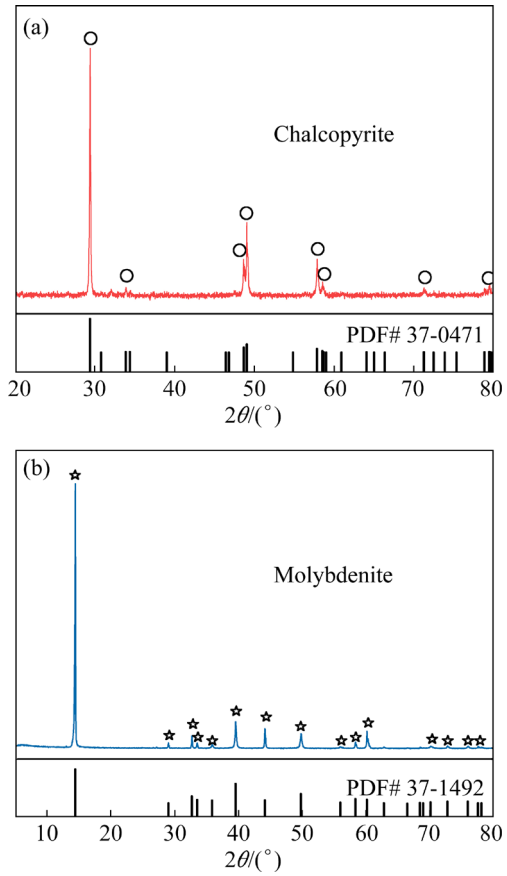

Fig. 2 XRD patterns of chalcopyrite (a) and molybdenite (b) samples

2.3 FT-IR analysis

Comparative investigations of the infrared spectra of chalcopyrite and molybdenite before and after reagent treatment were carried out. The diffuse reflectance mode (DRIFTS) was used to characterize the mineral samples by RAffinity-1S (Shimadzu Instruments, Japan) within the wavenumber range of 500−4000 cm^{-1}. For this purpose, 2.0 g of each mineral sample was pulverized to obtain a particle size of 5 μm in the agate mortar and then mixed with 100 mL of collector solution for 4 min. The solid fraction was filtered, washed with DI water (pH (7±0.2)), dried at 90 ℃ for 1 h, and then analyzed.

2.4 XPS measurements

XPS analyses were performed with an Escalab 250 Xi energy spectrometer using a focused monochromatized Al K_α radiation (Leica, Holland). The acceleration voltage and the applied current were 40 kV and 25 mA, respectively. The binding energy scale was calibrated from the carbon contamination (always present at the material surface) using the C 1s peak at 284.8 eV. The test sample was prepared in the same way as the microflotation test.

2.5 AFM observation

The characterization of mineral surface topography before and after reagent treatment was detected using a multimode V atomic force microscopy (Bruker, USA) with a tapping mode in a nitrogen atmosphere at 25 °C. Samples were polished using a semi-automatic grinding and polishing machine (Buehler, USA), then sonicated with DI water and dried with N_2. After this, the final product was transferred to the AFM measurement.

3 Results and discussion

3.1 Microflotation experiments

The recovery of chalcopyrite and molybdenite as a function of TLA concentration in the presence of SBX at pH (7±0.2) is shown in Fig. 3. Note that

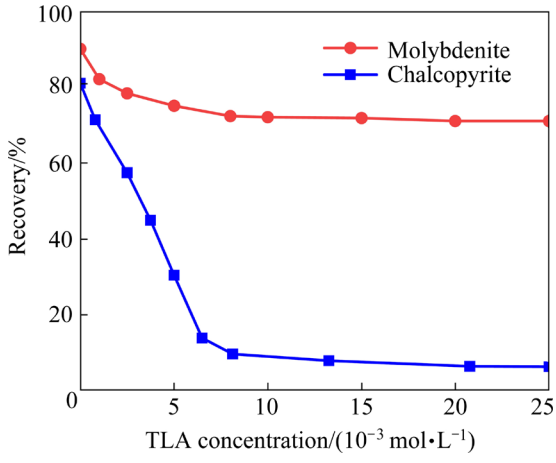

Fig. 3 Recoveries of chalcopyrite and molybdenum as function of TLA dosage in the presence of 4×10^{-4} mol/L SBX

TLA acts as an effective depressant for chalcopyrite in flotation. It was clear from Fig. 3 that chalcopyrite recovery steeply dropped from 81% to 9.7% as the concentration of TLA increased to 8×10^{-3} mol/L. Above this range, the chalcopyrite recovery did not change significantly. Therefore, 8×10^{-3} mol/L TLA was sufficient to depress chalcopyrite flotation. In contrast, the floatability of molybdenite was barely affected by TLA and remained above 71% over the entire TLA concentration range.

The effect of TLA on the separation of molybdenite from chalcopyrite was investigated using a microflotation experiment of artificial mixed molybdenite–chalcopyrite minerals. Figure 4(a_1, b_1) show that changes in TLA concentration did not affect molybdenite floatability, with chalcopyrite always being depressed. When 5×10^{-3} mol/L TLA was added to the mixtures (the mass ratios of chalcopyrite to molybdenite were 1:3 and 3:1), the chalcopyrite recovery was significantly decreased to 5.15% and 10.63% from 89.22% and 99.1%, respectively. In comparison, molybdenite recovery consistently fluctuated in the high-value range in the presence and absence of TLA. The Gaudin selectivity index was then established to describe the separation selectivity of TLA, as illustrated in Figs. 4(a_2, b_2). It can be seen that, the introduction of TLA greatly improved the SI of mixture minerals. As a result, adding TLA enhanced molybdenite separation efficiency substantially, suggesting a good selectivity of TLA for recovering molybdenite from chalcopyrite.

3.2 FT-IR analysis

Figure 5 shows the FT-IR spectra of SBX and TLA at pH (7±0.2). As shown, for SBX, the bands between 2958 and 2870 cm^{-1} were related to the C—H stretching of CH_3 and CH_2 groups [27]. The peaks between 1468 and 1116 cm^{-1} represented the stretching vibration of C—O—C [28]. In addition, the peak at 1059 cm^{-1} was attributed to the SBX characteristic group C═S [29,30]. As for TLA, these peaks at 2763 and 2574 cm^{-1} corresponded to

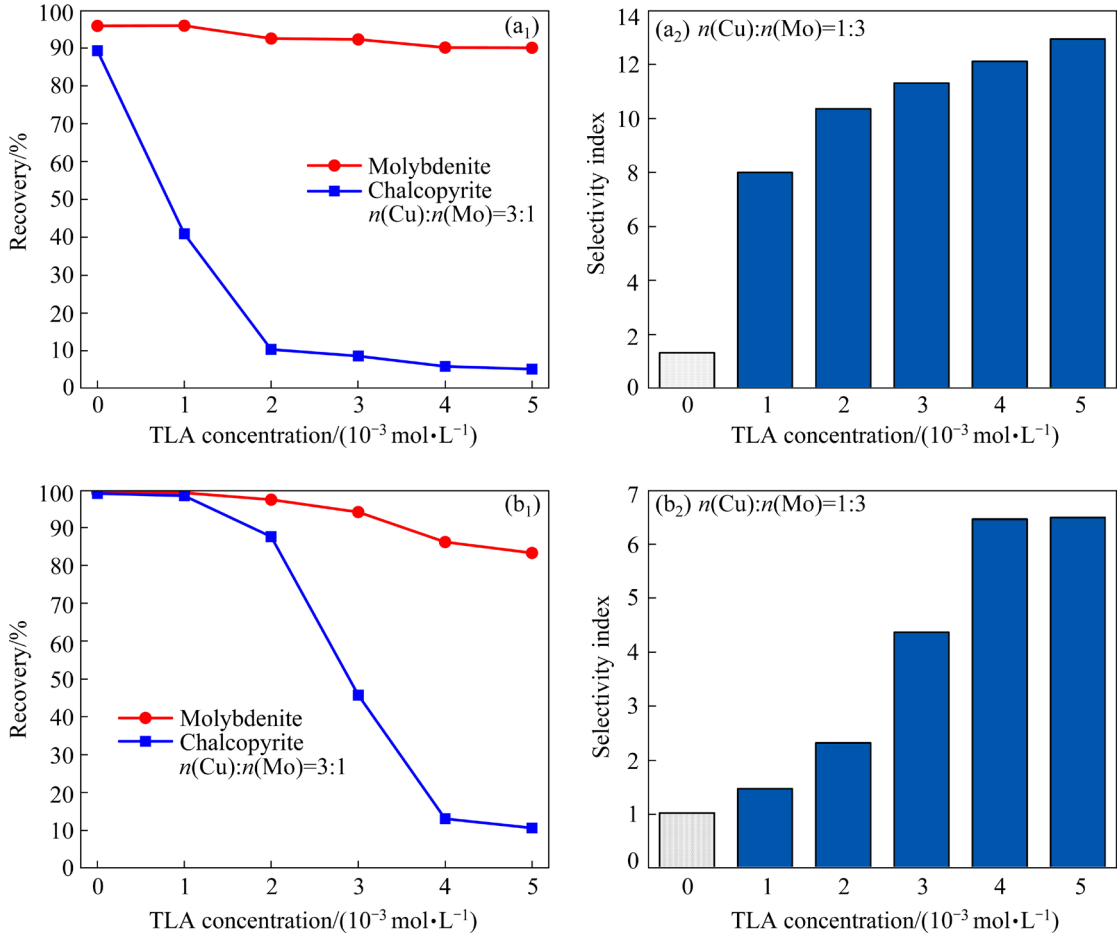

Fig. 4 Recovery (a_1, b_1) and selectivity index (a_2, b_2) of mixed minerals with mass ratios of chalcopyrite to molybdenite of 1:3 (a_1, a_2) and 3:1 (b_1, b_2) as function of TLA concentration

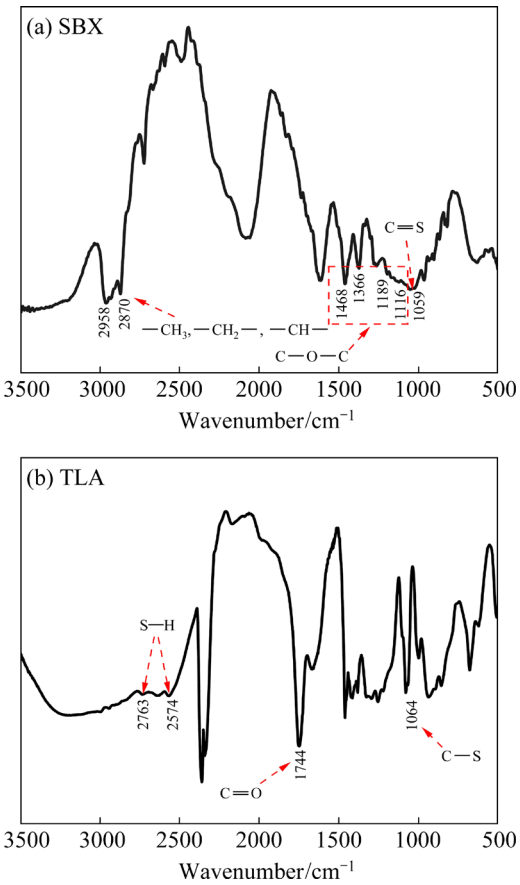

Fig. 5 FI-TR spectra of SBX (a) and TLA (b)

the S—H group [7], while other peaks at 1744 and 1064 cm^{-1} belonged to the C═O and C—S groups [31], respectively.

Figure 6 describes IR spectra of chalcopyrite before and after treatment with SBX and TLA. As depicted in Fig. 6(b), with treatment of SBX, the stretching vibration of C—O—C emerged at 1269, 1192, and 1193 cm^{-1} on the chalcopyrite surface [32]. In addition, the peak of the C═S stretching vibration was shifted from 1059 to 1024 cm^{-1}. These changes confirmed that SBX was chemically adsorbed on the chalcopyrite through the C═S and C—O—C functional groups.

In Fig. 6(c), FTIR spectra of TLA-treated chalcopyrite showed possible adsorption of TLA on the chalcopyrite surface at approximately 1685 and 3547−3815 cm^{-1}, both corresponding to the carboxylate group stretching. Furthermore, the bonds attributed to S — H groups (2763 and 2574 cm^{-1}) of TLA disappeared. These results suggested that TLA may be adsorbed on the surface of chalcopyrite in two ways. The one is electrostatic adsorption between TLA and the surface product of chalcopyrite oxidation. The other is chemisorption between TLA and chalcopyrite through the S—H functional group.

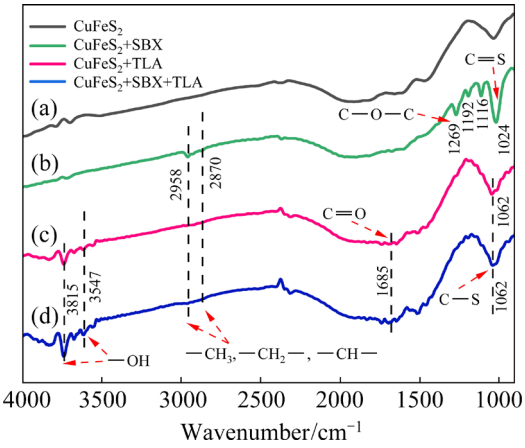

Fig. 6 FTIR spectra of chalcopyrite before and after reagent treatment

Figure 6(d) indicates the IR spectra of chalcopyrite interacted with TLA and SBX sequentially. The characteristic peaks of SBX disappeared and were replaced by the carboxylate group stretching and C—S function group of TLA. TLA showed a strong competitive adsorption effect towards SBX on the chalcopyrite surface. It preferentially occupied the active sites on the chalcopyrite surface, resulting in the inability of SBX to chemisorb on the chalcopyrite surface.

As for molybdenite (Fig. 7), when interacted with SBX, the stretching vibration peaks of C—H and C—O—C bonds appeared at 2958−2870 cm^{-1} and 1465−1118 cm^{-1}, respectively. The characteristic of C═S was shifted from 1059 to 1031 cm^{-1}. This confirmed the strong adhesion of SBX on the molybdenite surface.

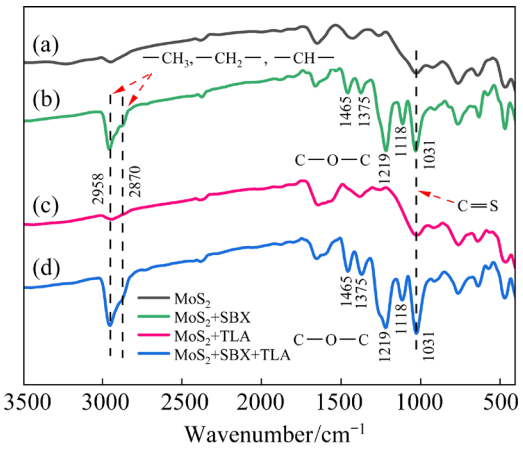

Fig. 7 FTIR spectra of molybdenite before and after reagent treatment

As shown in Figs. 7(c, d), there were no obvious changes in the IR spectra of TLA-treated molybdenite. The peaks of C—O—C and C═S belonging to SBX still existed in the IR spectra of TLA−SBX-treated molybdenite. These phenomena indicated that TLA was weakly adsorbed onto molybdenite, which barely affected the subsequent SBX adhesion on the molybdenite surface. Accordingly, chalcopyrite flotation was selectively depressed.

3.3 XPS analysis

The XPS analysis was used to investigate the chemical state variation on the mineral surfaces. Here, XPS analysis was used to further investigate the selective depression mechanism of TLA in the flotation separation of chalcopyrite and molybdenite.

Figure 8 demonstrates the high-resolution spectra of C 1s on chalcopyrite before and after reagent treatment. In natural chalcopyrite, the C 1s consisted of three peaks at 284.8, 286.3, and 288.8 eV, which could be assigned to C — C, C—O—C, and C═O [33−35], respectively. As seen in Fig. 8(b), a comparison of binding energy of C 1s obtained from chalcopyrite before and after SBX treatment indicated the higher peak intensity of C—O—C on SBX-treated chalcopyrite surface, which was attributed to interaction between SBX and chalcopyrite via the C—O—C function groups. TLA also exhibited strong chemical adsorption on the chalcopyrite surface, as evidenced by the decrease in C═O peak intensity from 288.8 to 288.4 eV in Fig. 8(c). Figure 8(d) showed that the binding energy shifts of the C═O peak still existed, and C—O—C binding energy shifts disappeared on the chalcopyrite surface. This observation might be ascribed to the hypothesis of the adsorption mechanism that TLA preferentially occupied the active site on the chalcopyrite surface, suppressing SBX chemisorption on the chalcopyrite surface.

Figure 9 shows Cu 2p core peaks of natural, SBX-treated, TLA-treated, and TLA−SBX-treated chalcopyrite. As previously reported [36,37], the original chalcopyrite Cu 2p spectrum could be fitted with two peaks at 932.07 and 951.9 eV, corresponding to $CuFeS_2$ and $Cu(OH)_2$, respectively. After treatment with SBX (Fig. 9(b)) and TLA (Fig. 9(c)), the peaks of $CuFeS_2$ were shifted by 0.37 eV to a much lower binding energy of 931.7 eV, owing to the electron from certain groups of SBX and TLA. This phenomenon also appeared on the TLA−SBX-treated chalcopyrite surface. It is likely that chemical adsorption occurred on the chalcopyrite surface between the Cu atom of chalcopyrite and reagents.

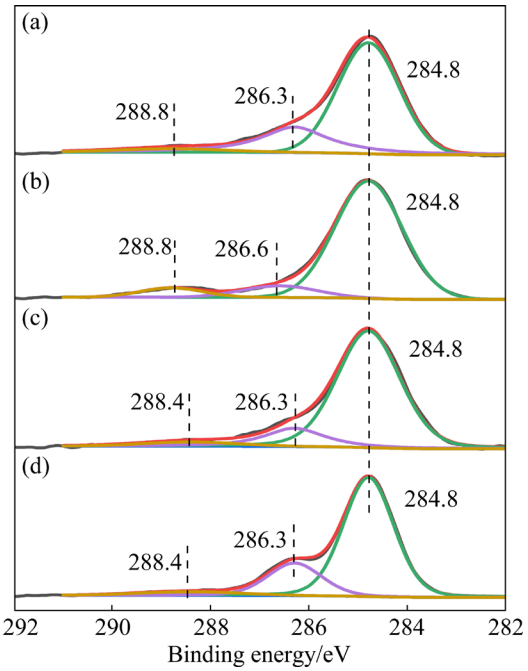

Fig. 8 C 1s XPS spectra of chalcopyrite (a), SBX-treated chalcopyrite (b), TLA-treated chalcopyrite (c), and TLA−SBX-treated chalcopyrite (d)

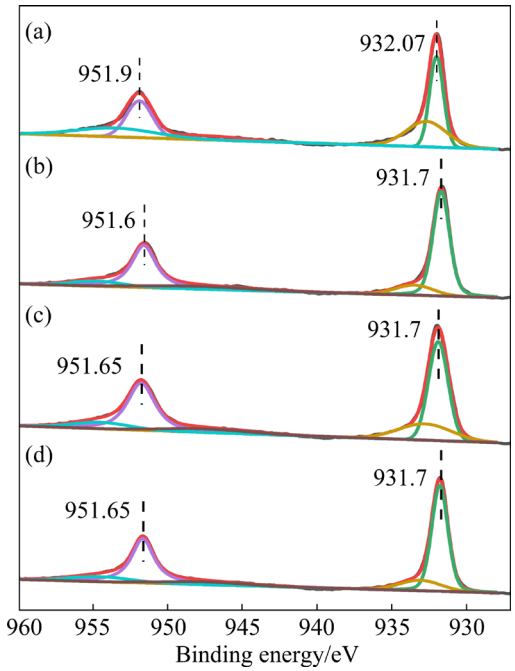

Fig. 9 Cu 2p XPS spectra of chalcopyrite (a), SBX-treated chalcopyrite (b), TLA-treated chalcopyrite (c), and TLA−SBX-treated chalcopyrite (d)

In the S 2p spectra of chalcopyrite (Fig. 10), the peaks at 161.1, 162.3, 163.21, and 164.3 eV could be assigned to S^{2-}, S_2^{2-}, S_n^{2-}/S^0, and energy loss [38,39], respectively. When SBX was added, two new peaks at 161.85 and 164.8 eV contributed to C—S [40] and C═S [41] functional groups, suggesting the chemisorption between SBX and chalcopyrite. After adding TLA, the new peak at 164.08 eV corresponded to the —SH species from TLA. After TLA modified the chalcopyrite surface in the presence of SBX, the peak located at 164.25 eV corresponded to the —SH functional group of TLA, and the C═S and C—S peaks belonging to SBX disappeared. These results demonstrated that TLA preferentially adsorbed on the chalcopyrite surface via the —SH functional group, thus preventing the adsorption of SBX.

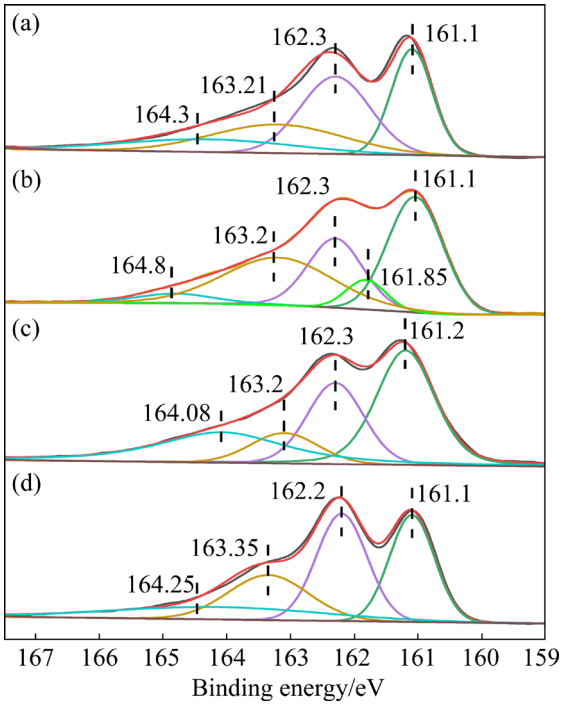

Fig. 10 S 2p XPS spectra of chalcopyrite (a), SBX-treated chalcopyrite (b), TLA-treated chalcopyrite (c), and TLA−SBX-treated chalcopyrite (d)

Figure 11 shows the precise scan of the C 1s core peaks of natural, SBX-treated, TLA-treated, and SBX-treated molybdenite in the presence of TLA. As seen in Fig. 11(a), the peak fitting of the C 1s spectrum of natural molybdenite gave three peaks at 288.85, 286.05, and 284.8 eV, attributing to the C═O, C—O—C, and C—C [42], respectively. It could be observed that the binding energy of C—O—C (286.33 eV) in SBX-treated molybdenite was increased by 0.28 eV, suggesting the chemisorption between SBX and molybdenite. No significant binding energy shift of C═O and C—O—C occurred on TLA-treated molybdenite surface, demonstrating that TLA had negligible influence on the chemical state of the C atom. The binding energy of C—O—C in the molybdenite surface prepared by SBX and TLA was shifted from 286.05 to 286.45 eV, an increase of 0.4 eV compared to natural molybdenite due to the still existing chemisorption of SBX on the chalcopyrite surface.

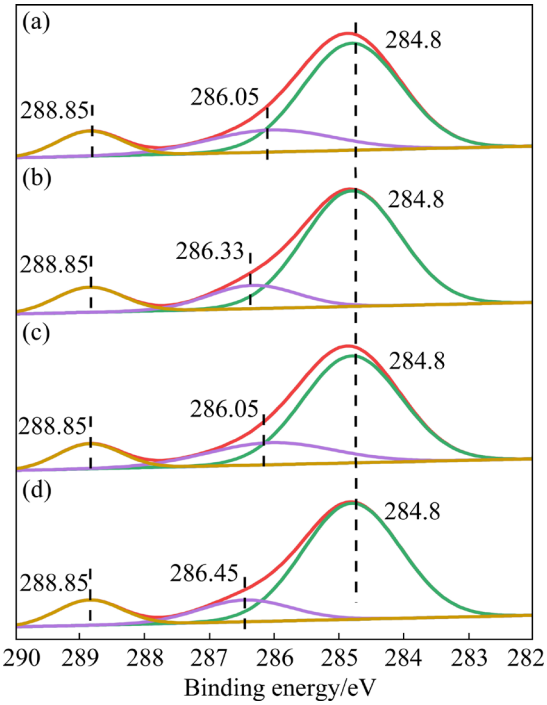

Fig. 11 C 1s XPS spectra of molybdenite (a), SBX-treated molybdenite (b), TLA-treated molybdenite (c), and TLA−SBX-treated molybdenite (d)

In the Mo 3d spectra (Fig. 12), the peaks located at 233.17 and 230.02 eV could be assigned to Mo $3d_{5/2}$ and Mo $3d_{3/2}$ of natural molybdenite [41], respectively. After the addition of SBX, the peaks of Mo $3d_{5/2}$ and Mo $3d_{3/2}$ were shifted by 0.53 and 0.48 eV, respectively, suggesting that the Mo atom might participate in the interaction between SBX and molybdenite. As shown in the Mo 3d spectra of TLA-treated molybdenite, no significant binding energy shift (<0.1 eV) occurred. In contrast, the binding energy of Mo $3d_{5/2}$ and Mo $3d_{3/2}$ peaks were shifted by 0.55 and 0.53 eV in TLA−SBX-treated molybdenite. These results demonstrated no significant inhibition

of TLA on the molybdenite in the flotation with and without the presence of SBX.

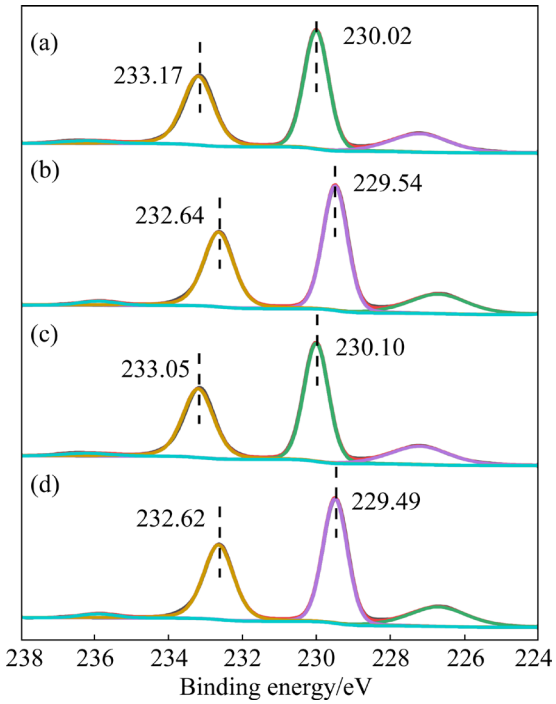

Fig. 12 Mo 3d XPS spectra of molybdenite (a), SBX-treated molybdenite (b), TLA-treated molybdenite (c), and TLA−SBX-treated molybdenite (d)

3.4 AFM measurement

All of the AFM testing scan range was set at 1 μm × 1 μm. Figure 13 illustrates the 3D and 2D images of the studied minerals. The left images are 3D images, which can be used to visually observe the morphology features of the mineral surface. The right image represents a height image with different colors, indicating different mineral surface heights.

Figure 13(a) indicates homogeneous distribution of the chalcopyrite surface with a root mean square (RMS) roughness (R_q) of 1.83 nm. The AFM image of the SBX-treated chalcopyrite is shown in Fig. 13(b). It can be seen that, the R_q of the chalcopyrite surface was shifted to 4.70 from 1.83 nm, and SBX exhibited uniform patches on the chalcopyrite surface. As shown in Fig. 13(c), the R_q of TLA-treated chalcopyrite increased from 1.83 to 2.05 nm, and the linear stratification on the chalcopyrite surface vanished. Figure 13(d) shows that the R_q of TLA−SBX-treated chalcopyrite decreased from 4.70 to 1.80 nm, and the adsorbed batches of SBX disappeared. Thus, TLA strongly inhibited SBX adsorption on the chalcopyrite surface, consistent with the FTIR and XPS analyses.

Figure 14 illustrates the surface morphology of molybdenite before and after reagent treatment. The flat molybdenite surface was confirmed by its well-cleaved state in Fig. 14(a). SBX exhibited uniform point-like adsorption on the SBX-treated molybdenite surface, similar to the SBX-treated chalcopyrite. In contrast, no TLA accumulation was visible on the AFM image of TLA-treated molybdenite. When molybdenite reacted with TLA and SBX, the R_q of 5.32 nm molybdenite surface illustrated that SBX could still chemisorb on the molybdenite surface in the presence of TLA.

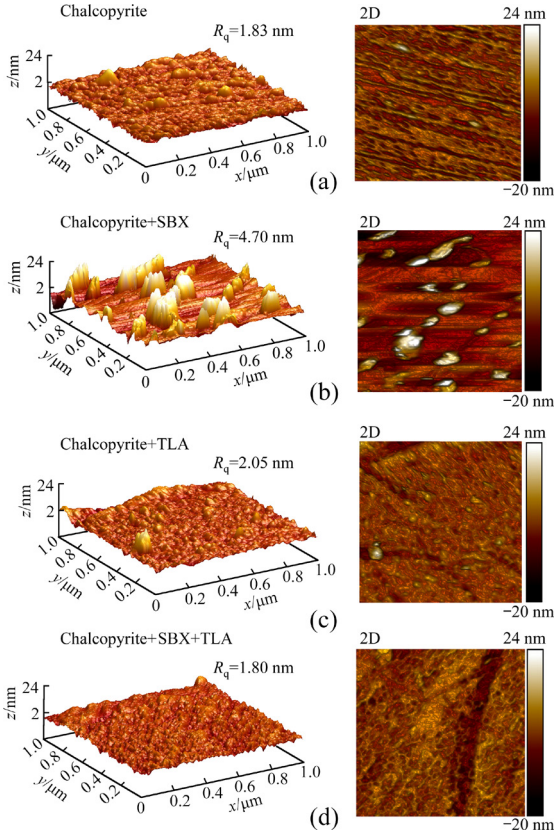

Fig. 13 AFM images of chalcopyrite before and after reagent treatment

3.5 Adsorption mechanism and model analysis

Based on the above analyses, a possible adsorption model of TLA on the chalcopyrite surface is indicated in Fig. 15. Through the —SH and —COOH groups, TLA preferentially occupied the active sites on the chalcopyrite surface, suppressing the subsequent SBX adsorption on the chalcopyrite surface. On the other hand, TLA did not cling to the surface of molybdenite, which made it easier to separate molybdenite and chalcopyrite.

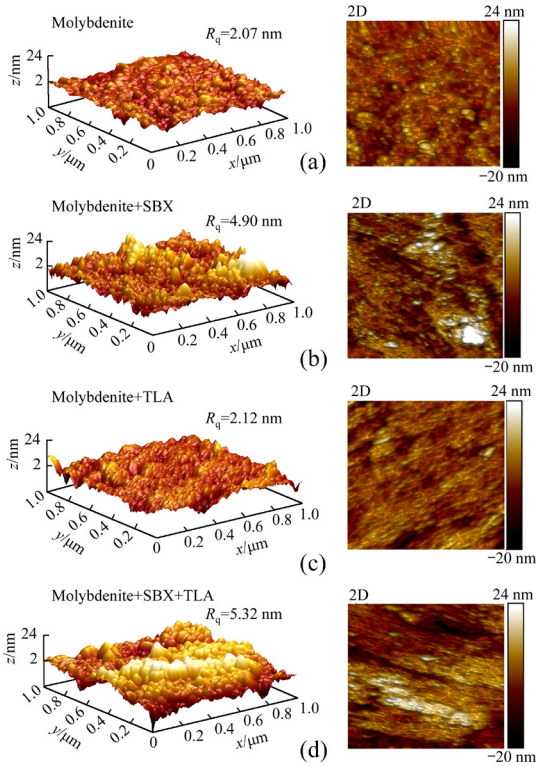

Fig. 14 AFM images of molybdenite before and after treatment with reagents

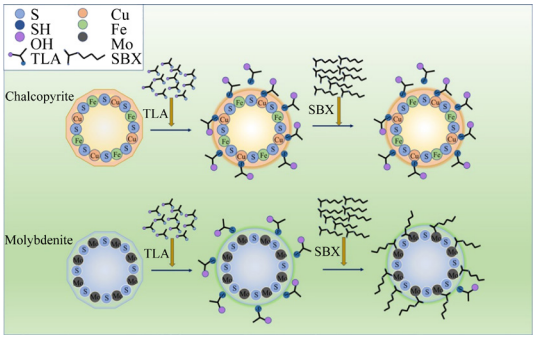

Fig. 15 Proposed adsorption model of TLA on mineral surface

4 Conclusions

(1) TLA was a non-toxic and highly efficient organic chalcopyrite depressant. It could be considered a practical alternative depressant to separate molybdenite from chalcopyrite in flotation.

(2) In the flotation system consisting of TLA and SBX, chalcopyrite recovery decreased from 81% to 9.7%, while the recovery of molybdenite remained around 71%. Meanwhile, a good Gaudin selectivity index of 12.9 and 6.5 was obtained in the artificial mixed minerals flotation of different mass ratios of these two minerals (n(Cu):n(Mo)=1:3 and n(Cu):n(Mo)=3:1).

(3) FT-IR, XPS, and AFM analysis revealed that the chemisorption of TLA was strong on chalcopyrite surface through —SH and —COOH groups but weak on molybdenite surface, which can hinder the further chemisorption of SBX on chalcopyrite surface.

Acknowledgments

This research was funded by the National Key R&D Program of China (No. 2022YFC2904501), the National Natural Science Foundation of China (Nos. 52004335, 52004337), the Natural Science Foundation of Hunan Province, China (No. 2023JJ20071), the Science and Technology Innovation Program of Hunan Province, China (No. 2023RC3067), and the Key Laboratory of Hunan Province for Clean and Efficient Utilization of Strategic Calcium-containing Mineral Resources, China (No. 2018TP1002).

References

[1] WEI Han, YANG Hao-yu, ZHANG Xiao-qi, ZHU Jian-feng, QIU Peng-peng, LUO Wei. Hydrogen peroxide enabled two-dimensional molybdenum trioxide nanosheet clusters for enhanced surface Li-ion storage [J]. Tungsten, 2021, 3: 338−347.

[2] GENG Kun-qi, YANG Meng-qian, MENG Jun-xia, ZHOU Ling-fei, WANG Yu-qin, DMYTRO S, ZHANG Qian, ZHONG Sheng-wen, MA Quan-xin. Engineering layered/spinel heterostructure via molybdenum doping towards highly stable Li-rich cathodes [J]. Tungsten, 2022, 4: 323−335.

[3] ZHANG Xing-lai, LI Jing, LENG Bing, YANG Liu, SONG Yan-dong, FENG Si-yu, FENG Li-zhi, LIU Zi-tong, FU Zheng-wei, JIANG Xin, LIU Bao-dan. High-performance ultraviolet-visible photodetector with high sensitivity and fast response speed based on MoS_2-on-ZnO photogating heterojunction [J]. Tungsten, 2023, 5: 91−99.

[4] ZENG Jian, XU Liang, LUO Xin, CHEN Tong, TANG Shuai-hao, HUANG Xin, WANG Liang-liang. Z-scheme systems of ASi_2N_4 (A = Mo or W) for photocatalytic water splitting and nanogenerators [J]. Tungsten, 2022, 4: 52−59.

[5] YUAN Duo-wei, CADIEN K, LIU Qi, ZENG Hong-bo. Separation of talc and molybdenite: Challenges and opportunities [J]. Minerals Engineering, 2019, 143: 105923.

[6] DUTTA S K, LODHARI D R. Topics in mining, metallurgy and materials engineering [M]. Springer Science and Business Media Deutschland GmbH, 2018, 205−209.

[7] CHEN Yang, CHEN Xu-ming, PENG Yong-jun. The effect of sodium hydrosulfide on molybdenite flotation as a depressant of copper sulfides [J]. Minerals Engineering, 2020, 148: 106203.

[8] LIN Qing-quan, GU Guo-hua, WANG Hui, LIU You-cai, FU Jian-gang, ZHAO Jun-yao, HUANG Luo-luo. Recovery of molybdenum and copper from porphyry ore via

iso-flotability flotation [J]. Transactions of Nonferrous Metals Society of China, 2017, 27: 2260−2271.

[9] LIU Run-qing, LI Jie, SONG Xin, WANG Chang-tao, CHEN Chen, ZHANG Qing-peng, SUN Wei. Enhancing mechanism and application on flotation of molybdenites with different particle size by using compound hydrocarbon oil [J]. The Chinese Journal of Nonferrous Metals, 2023, 33(3): 912−921. (in Chinese)

[10] YANG Bing-qiao, Wang De-ru, WANG Tian-shuai, ZHANG Han-quan, JIA Fei-fei, SONG Shao-xian. Effect of Cu^{2+} and Fe^{3+} on the depression of molybdenite in flotation [J]. Minerals Engineering, 2019, 130: 101−109.

[11] LI Ming-yang, WEI De-zhou, LIU Qi, LIU Wen-bao, ZHENG Ji-min. SUN Hong-jie. Flotation separation of copper-molybdenum sulfides using chitosan as a selective depressant [J]. Minerals Engineering, 2015, 83: 217−222.

[12] YAN Hai, YANG Bing-qiao, ZENG Meng-yuan, FENG Ji-chan, ZHU Huan-yu. Application and mechanism of ammonium persulfate in separation of copper−molybdenum sulfide [J]. The Chinese Journal of Nonferrous Metals, 2022, 32(1): 279−285. (in Chinese)

[13] YIN Zhi-gang, SUN Wei, HU Yue-hua, ZHANG Chen-hu, GUAN Qing-jun, LIU Run-qing, CHEN Pan, TIAN Meng-jie, Utilization of acetic acid-[(hydrazinylthio-xomethyl)thio]-sodium as a novel selective depressant for chalcopyrite in the flotation separation of molybdenite [J]. Separation and Purification Technology, 2017, 179: 248−256.

[14] ANSARI A, PAWLIK M. Floatability of chalcopyrite and molybdenite in the presence of lignosulfonates. Part II: Hallimond tube flotation [J]. Minerals Engineering, 2007, 20: 609−616.

[15] PEARSE M J. An overview of the use of chemical reagents in mineral processing [J]. Minerals Engineering, 2005, 18: 139−149.

[16] YUAN Duo-wei, CADIEN K, LIU Qi, ZENG Hong-bo. Selective separation of copper−molybdenum sulfides using humic acids [J]. Minerals Engineering, 2019, 133: 43−46.

[17] SUYANTARA G P W, HIRAJIMA T, MIKI H, SASAKI K, YAMANE M, TAKIDA E, KUROIWA S, IMAIZUMI Y. Effect of Fenton-like oxidation reagent on hydrophobicity and floatability of chalcopyrite and molybdenite [J]. Colloids and Surfaces A: Physicochemical and Engineering Aspects, 2018, 554: 34−48.

[18] ZHAO Qiang, LIU Wen-gang, WEI De-zhou, WANG Wen-dan, CUI Bao-yu, LIU Wen-bao. Effect of copper ions on the flotation separation of chalcopyrite and molybdenite using sodium sulfide as a depressant [J]. Minerals Engineering, 2018, 115: 44−52.

[19] PARK I, HONG S, JEON S, ITO M, HIROYOSHI N. A review of recent advances in depression techniques for flotation separation of Cu-Mo sulfides in porphyry copper deposits [J]. Metals (Basel), 2020, 10(9): 1269.

[20] YIN Zhi-gang, CHEN Sheng-da, XU Zhi-jie, ZHANG Chen-yang, HE Jian-yong, ZOU Jing-xiang, CHEN Dai-xiong, SUN Wei. Flotation separation of molybdenite from chalcopyrite using an environmentally-efficient depressant L-cysteine and its adsoption mechanism [J]. Minerals Engineering, 2020, 156: 106438.

[21] YUAN Duo-wei, CADIEN K, LIU Qi, ZENG Hong-bo. Adsorption characteristics and mechanisms of O-carboxymethyl chitosan on chalcopyrite and molybdenite [J]. Journal of Colloid and Interface Science, 2019, 552: 659−670.

[22] YAN Hai, YANG Bing-qiao, ZENG Meng-yuan, HUANG Peng-liang, TENG Ii-ping. Selective flotation of Cu−Mo sulfides using xanthan gum as a novel depressant [J]. Minerals Engineering, 2020, 156: 106486.

[23] LIU Y, LIU Q. Flotation separation of carbonate from sulfide minerals, II: Mechanisms of flotation depression of sulfide minerals by thioglycollic acid and citric acid [J]. Minerals Engineering. 2004, 17: 865−878.

[24] ELIZONDO-ÁLVAREZ M A, URIBE-SALAS A, BELLO-TEODORO S. Chemical stability of xanthates, dithiophosphinates and hydroxamic acids in aqueous solutions and their environmental implications [J]. Ecotoxicology and Environmental Safety, 2021, 207: 111509.

[25] SHEN Yang, NAGARAJ D R, FARINATO R, SOMASUNDARAN P. Study of xanthate decomposition in aqueous solutions [J]. Minerals Engineering, 2016, 93: 10−15.

[26] NURI O S, ALLAHKARAMI E, IRANNAJAD M, ABDOLLAHZADEH A. Estimation of selectivity index and separation efficiency of copper flotation process using ANN model [J]. Geosystem Engineering, 2017, 20(1): 41−50.

[27] ZHONG Chun-hui, WANG Hui-hui, ZHANG Liang-zhu, GUO Meng-chi, FENG Bo. Flotation separation of molybdenite and talc by xanthan gum [J]. Powder Technology, 2021, 388: 158−165.

[28] CHANDRA A P, PUSKAR L, SIMPSON D J, GERSON A R. Copper and xanthate adsorption onto pyrite surfaces: Implications for mineral separation through flotation [J]. International Journal of Mineral Processing, 2012, 114/115/116/117: 16−26.

[29] KHOSO S A, HU Yue-hua, LÜ Fei, GAO Ya, LIU Run-qing, SUN Wei. Xanthate interaction and flotation separation of H_2O_2-treated chalcopyrite and pyrite [J]. Transactions of Nonferrous Metals Society of China, 2019, 29: 2604−2614.

[30] ZHANG Qian, WANG Yi-jie, FENG Qi-cheng, WEN Shu-ming, ZHOU Yao-wen, NIE Wen-lin, LIU Jun-bo. Identification of sulfidization products formed on azurite surfaces and its correlations with xanthate adsorption and flotation [J]. Applied Surface Science, 2020, 511: 145594.

[31] JIMÉNEZ-HERNÁNDEZ L, ESTÉVEZ-HERNÁNDEZ O, HERNÁNDEZ-SÁNCHEZ M, DÍAZ J A, FARÍAS-SÁNCHEZ M, REGUERA E. 3-mercaptopropionic acid surface modification of Cu-doped ZnO nanoparticles: Their properties and peroxidase conjugation [J]. Colloids and Surfaces A: Physicochemical and Engineering Aspects, 2016, 489: 351−359.

[32] ZHONG Chun-hui, FENG Bo, YAN Hua-shan, ZHOU Ying, LIU Gang, CHEN Yuan-gan, NING Xiang-han, WANG Hui-hui. Effect of three organic depressants on flotation separation of molybdenite and talc [J]. The Chinese Journal of Nonferrous Metals, 2022, 32(12): 3843−3852. (in Chinese)

[33] LI Wan-qing, LI Yu-biao. Improved understanding of

chalcopyrite flotation in seawater using sodium hexametaphosphate [J]. Minerals Engineering, 2019, 134: 269−274.
[34] IKUMAPAYI F, MAKITALO M, JOHANSSON B, RAO K H. Recycling of process water in sulphide flotation: Effect of calcium and sulphate ions on flotation of galena [J]. Minerals Engineering, 2012, 39: 77−88.
[35] ZHONG Chun-hui, FENG Bo, CHEN Yuan-gan, GUO Meng-chi, WANG Hui-hui. Flotation separation of molybdenite and talc using tragacanth gum as depressant and potassium butyl xanthate as collector [J]. Transactions of Nonferrous Metals Society of China, 2021, 31: 3879−3890.
[36] YANG Bing-qiao, YAN Hai, Zeng Meng-yuan, HUANG Peng-liang, JIA Fei-fei, TENG Ai-ping. A novel copper depressant for selective flotation of chalcopyrite and molybdenite [J]. Minerals Engineering, 2020, 151: 106309.
[37] WANG Jun, GAN Xiao-Wen, ZHAO Hong-bo, HU Ming-hao, LI Kai-yu, QIN Wen-qing, QIU Guan-zhou. Dissolution and passivation mechanisms of chalcopyrite during bioleaching: DFT calculation, XPS and electrochemistry analysis [J]. Minerals Engineering, 2016, 98: 264−278.
[38] YANG Yi, HARMER S, CHEN Miao. Synchrotron-based XPS and NEXAFS study of surface chemical species during electrochemical oxidation of chalcopyrite [J]. Hydrometallurgy, 2015, 156: 89−98.
[39] YU Jin-sheng, LIU Run-qing, WANG Li, SUN Wei, PENG Hong, HU Yue-hua. Selective depression mechanism of ferric chromium lignin sulfonate for chalcopyrite–galena flotation separation [J]. International Journal of Minerals, Metallurgy and Materials, 2018, 25: 489−497.
[40] LIU Sheng, XIE Lei, LIU Guang-yi, ZHONG Hong, WANG Yi-xiang, ZENG Hong-bo. Hetero-difunctional reagent with superior flotation performance to chalcopyrite and the associated surface interaction mechanism [J]. Langmuir, 2019, 35(12): 4353−4363.
[41] GUAN Chang-ping, YIN Zhi-gang, KHOSO S A, SUN Wei, HU Yue-hua. Performance analysis of thiocarbonohydrazide as a novel selective depressant for chalcopyrite in molybdenite-chalcopyrite separation [J]. Minerals, 2018, 8(4): 142.
[42] HAN Shi-kui, KONG Ming-guang, GUO ying, WANG Ming-tai. Synthesis of copper indium sulfide nanoparticles by solvothermal method [J]. Materials Letters, 2009, 63(13/14): 1192−1194.
[43] YANG Bing-qiao, YAN Hai, ZENG Meng-yuan, ZHU Huan-yu. Tiopronin as a novel copper depressant for the selective flotation separation of chalcopyrite and molybdenite [J]. Separation and Purification Technology, 2021, 266: 118576.

硫代乳酸抑制剂分离辉钼矿与黄铜矿：浮选行为及机理

黄伟欣[1,2]，唐鸿鹄[1,2]，曹 杨[1,2]，刘若华[1,2]，孙 伟[1,2]

1. 中南大学 资源加工与生物工程学院，长沙 410083；
2. 中南大学 金属资源开发利用碳减排教育部工程研究中心，长沙 410083

摘 要：针对黄铜矿与辉钼矿可浮性相似导致分离难的问题，亟需开发一种经济与绿色的抑制剂。提出一种新型黄铜矿抑制剂硫代乳酸。通过单矿物和人工混合矿浮选实验，对硫代乳酸的浮选行为进行研究。单矿物浮选实验结果表明，硫代乳酸对黄铜矿具有较好的抑制效果，硫代乳酸作用后，黄铜矿浮选回收率从 81%下降至 9.7%，而辉钼矿浮选回收率仍保持在 71%以上。人工混合矿浮选实验表明，黄铜矿与辉钼矿分离效果较好，高登选择性指数为 12.9。采用 FT-IR、XPS 和 AFM 等方法研究硫代乳酸在辉钼矿和黄铜矿表面的反应机理，并提出可能的吸附模型。结果表明，硫代乳酸的—SH 和—COOH 基团优先占据黄铜矿表面活性铜位点，阻止丁基黄原酸钠在黄铜矿表面的化学吸附。

关键词：硫代乳酸；黄铜矿；黄铜矿抑制剂；铜钼分离

(Edited by Bing YANG)